Available online at www.sciencedirect.com

ScienceDirect

Journal of Magnesium and Alloys 7 (2019) 514–521

www.elsevier.com/locate/jma

Full Length Article

Thermoelectric transport behaviours of n-type Mg_2 (Si,Sn,Ge) quaternary solid solutions

Övgü Ceyda Yelgel[a,b,*], Celal Yelgel[a,b]

[a] *Recep Tayyip Erdogan University, Faculty of Engineering, Department of Materials Science and Nanotechnology Engineering, 53100, Rize, Turkey*
[b] *University of Manchester, School of Physics and Astronomy, M139PL, UK*

Received 17 March 2019; received in revised form 2 June 2019; accepted 5 June 2019
Available online 29 July 2019

Abstract

Mg_2X (X=Si, Sn, and Ge) based systems have attracted widespread attention owing to their various benefits in thermoelectric applications. In particular, to date, ternary Mg_2X based solid solutions have become one of the most widely investigated thermoelectric systems. However, the investigation of temperature varied thermoelectric properties of Mg_2X based quaternary systems is rather limited both theoretically and experimentally. Therefore, here, we report a rigorous theoretical work of thermoelectric properties for n-type $Mg_2Si_{0.55-z}Sn_{0.4}Ge_{0.05}Bi_z$ quaternary solid solutions ($z=0.02$, 0.025, 0.03, and 0.035) from 300 K to 850 K. By using nearly-free-electron model together with Fermi–Dirac statistics we define Fermi level both in extrinsic and intrinsic regimes as a function of temperature. We follow Hicks and Dresselhaus' approach to calculate electronic transport properties. By performing the Debye's isotropic continuum model a detailed theoretical investigation of lattice thermal conductivity is presented among with various phonon relaxation rates. From our theoretical analysis the highest *ZT* is attained for $Mg_2Si_{0.53}Sn_{0.4}Ge_{0.05}Bi_{0.02}$ solid solution as 1.14 at 850 K.

© 2019 Published by Elsevier B.V. on behalf of Chongqing University.
This is an open access article under CC BY-NC-ND license. (http://creativecommons.org/licenses/by-nc-nd/4.0/)
Peer review under responsibility of Chongqing University

1. Introduction

Thermoelectric devices could convert various kinds of heat (i.e, solar heat, geothermal heat and exhaust gases of automobiles) into electricity and vice-versa. In recent years, thermoelectric devices are being paid more and more attention owing to their unique advantages such as no noise, less maintenance, no moving parts, and long life [1–5]. Dimensionless figure of merit *ZT* of thermoelectric materials is usually used to evaluate the conversion efficiency of a device. It is determined by combining transport properties of Seebeck coefficient (*S*), electrical conductivity (σ), and total thermal conductivity (κ_{total}) as

$$ZT = \frac{S^2\sigma}{\kappa_{total}}T, \quad (1)$$

where $\kappa_{total} = \kappa_c + \kappa_{bp} + \kappa_{ph}$ with carrier, bipolar, and phonon components of thermal conductivity, respectively. To design a thermoelectric device with enhanced value of *ZT* one seeks materials that have large Seebeck coefficient, are good conductors of electricity whereas are poor conductors of heat [1–5]. This is quite challenging task since all these three transport parameters are coupled to each other in classical physics. There are inverse relationships between σ and κ_c due to the Wiedemann Franz law and *S* and σ owing to the Boltzmann's transport theory. The most common strategy to maximize the *ZT* is to find new bulk materials and their further engineering to make them with efficiencies comparable to the current mechanical engines [1–5]. Semiconductors are very good thermoelectric materials and their performance can be further improved by choosing the best dopant and substitution to

* Corresponding author at: Recep Tayyip Erdogan University, Faculty of Engineering, Department of Materials Science and Nanotechnology Engineering, 53100, Rize, Turkey.
E-mail addresses: oceyda.yelgel@erdogan.edu.tr (Ö.C. Yelgel), celal.yelgel@erdogan.edu.tr (C. Yelgel).

https://doi.org/10.1016/j.jma.2019.06.001
2213-9567/© 2019 Published by Elsevier B.V. on behalf of Chongqing University. This is an open access article under CC BY-NC-ND license. (http://creativecommons.org/licenses/by-nc-nd/4.0/) Peer review under responsibility of Chongqing University

the correct site. Among all other alternative thermoelectrics working at 400 K $\leqslant T \leqslant$ 800 K (i.e PbTe or $CoSb_3$) the constituent elements of Mg_2X (X=Si, Sn, and Ge) compounds are of ascending interest due to their competitive advantages such as being low cost, non-toxicity, and abundant in nature, having low material density and tailorable electronic structures [1–6]. These Mg_2X based materials have narrow indirect band gaps and crystallize in anti-fluorite structure with space group $FM\bar{3}m$ having face centred cubic lattice [7–10]. They have been extensively studied in thermoelectric research society due to their attractive characteristics such as high Seebeck coefficient and electrical conductivity with small thermal conductivity which could be very useful for high performance thermoelectric applications [1–6,11–13]. The thermoelectric efficiency of Mg_2Si can be greatly improved by alloying with Mg_2Sn. Among the Mg_2(Si,Sn) ternary series, the Sn-rich members exhibit high ZT when doped with Sb and the work done by Zaitsev et al. was shown that n-type compositions of $Mg_2Si_{1-x}Sn_x$ with x =0.4 and x =0.6 had $ZT \backsim 1.1$ at $\backsim 800$ K [8]. Also, Liu et al. investigated $Mg_2Si_{1-x}Sn_x$ ($0.2 \leq x \leq 0.8$) and reported that the compositions with x =0.6 to x =0.7 had a maximum $ZT \backsim 1.3$ at $\backsim 750$ K [14]. The reason of having large ZT values of these systems is because of their significantly low thermal conductivity coming from enhanced short wave-length phonon scattering due to point defects. As a next stage of these studies nowadays quaternary Mg_2(Si, Sn, Ge) systems have attracted a great deal of attention due to their higher thermoelectric performances than their ternary series sourced from introducing additional atoms in the lattice. However, in thermoelectric research area the investigation of thermoelectric transport properties of Mg_2(Si, Sn, Ge) quaternary systems is still rare both theoretically and experimentally. In particular, there is an urgent need of a systematic and rigorous theoretical explanation for thermoelectric properties of these quaternary systems. Lately, from the experimental work of by Khan et al. [15] it was found that Bi doped $Mg_2Si_{1-x-y}Sn_xGe_y$ solid solution (x =0.4, y=0.05) exhibited very good thermoelectric performance with ZT=1.4 at 823 K. Therefore, in this research, we theoretically investigated quaternary n-type doped $Mg_2Si_{1-x-y-z}Sn_xGe_yBi_z$ solid solutions (with x=0.4, y=0.05, z=0.02, 0.025, 0.03, and 0.035) in terms of thermoelectric transport behaviours among with their experimental work reported by Khan et al. [15]. Being different from lots of theoretical works done so far [16–21] we assume the energy-dependent relaxation time assumption for thermoelectric transport properties since the energy-dependent acoustic phonon scattering mechanism plays an important role for Mg_2X based compounds [22,23]. Based on our theoretical model on temperature variant Fermi level [24] we calculate S, σ, and κ_c as a function of temperature with Hicks and Dresselhaus' approach [25]. Bipolar and phonon components of thermal conductivity are inserted by following Price's theory [26] and Debye's isotropic continuum model, respectively. Several phonon scattering processes are taken into account rigorously for our theoretical work to figure out dominantly effective phonon scattering mechanism for Mg_2(Si, Sn, Ge) quaternary systems.

2. Theory

First of all, we perform first-principles calculations using density functional theory (DFT) as implemented in the plane-wave-based Quantum ESPRESSO package [27]. We use the Perdew–Zunger exchange correlation corresponding to the local density approximation (LDA) [28]. We set the kinetc energy cutoffs of 120 Ry for the plane sets of Mg_2Si, $Mg_2Si_{0.55}Sn_{0.40}Ge_{0.05}$ and $Mg_2Si_{0.53}Sn_{0.40}Ge_{0.05}Bi_{0.02}$ structrues. The Brillouin zone is sampled using Γ-centred uniform Monkhorst–Pack [29] meshes with dimensions of $4 \times 4 \times 4$ (ionic relaxations) and $6 \times 6 \times 6$ (self-consistent field solutions). We fully relax all the structures until the maximum Hellmann–Feynman force acting on each atoms is smaller than 0.001 eV/Å. The total energy convergence is set to less than 10^{-8} eV in our calculations. A Methfessel–Paxton smearing [30] of 0.005 Ry is adopted in all calculations. We used $3 \times 3 \times 3$ supercell geometry of Mg_2Si using experimental lattice constant of Mg_2Si, 6.391 Å [31] to build $Mg_2Si_{0.55}Sn_{0.40}Ge_{0.05}$ and $Mg_2Si_{0.53}Sn_{0.40}Ge_{0.05}Bi_{0.02}$ structures. We randomly choose the substitution sites at each specific composition considering the structure with the highest symmetry. We carefully optimise the constructed $Mg_2Si_{0.55}Sn_{0.40}Ge_{0.05}$ and $Mg_2Si_{0.53}Sn_{0.40}Ge_{0.05}Bi_{0.02}$ structures which are shown in Fig. 1.

Theoretical calculations for thermoelectric transport properties are performed by assuming single band materials. In most of the previous works, the constant relaxation time approximation is generally used for thermoelectric properties calculations [16–21]. However, in this present work, we employ energy-dependent relaxation time approximation to present more accurate theoretical method. In our theoretical method for the thermoelectric transport properties the first step is to define temperature varied Fermi level both in extrinsic and intrinsic regimes. Within the single-band nearly-free-electron theory we follow Hicks and Dresselhaus' approach [25] to define S, σ, and κ_c as a function of temperature. The bipolar contribution on thermal conductivity (κ_{bp}) is calculated by following the Price's theory [26] with the simplified version of Glassbrenner and Slack's expression [32]. Lastly, we perform our lattice thermal conductivity calculations following the Debye's isotropic continuum model assuming single-mode relaxation time approach. Phonon relaxation rates contributed by boundary, mass defects, acoustic deformation potential, and anharmonic phonon scatterings are included rigorously. The expressions for electronic and thermal transport properties are listed in Table. 1.

3. Results and discussion

In this present work, theoretical calculations of thermoelectric transport properties are performed for $Mg_2Si_{0.55-z}Sn_{0.4}Ge_{0.05}Bi_z$ solid solutions with the doping level choosing as z=0.02, 0.025, 0.03, and 0.035, respectively. Parameters used for theoretical computations are listed in Table 2.

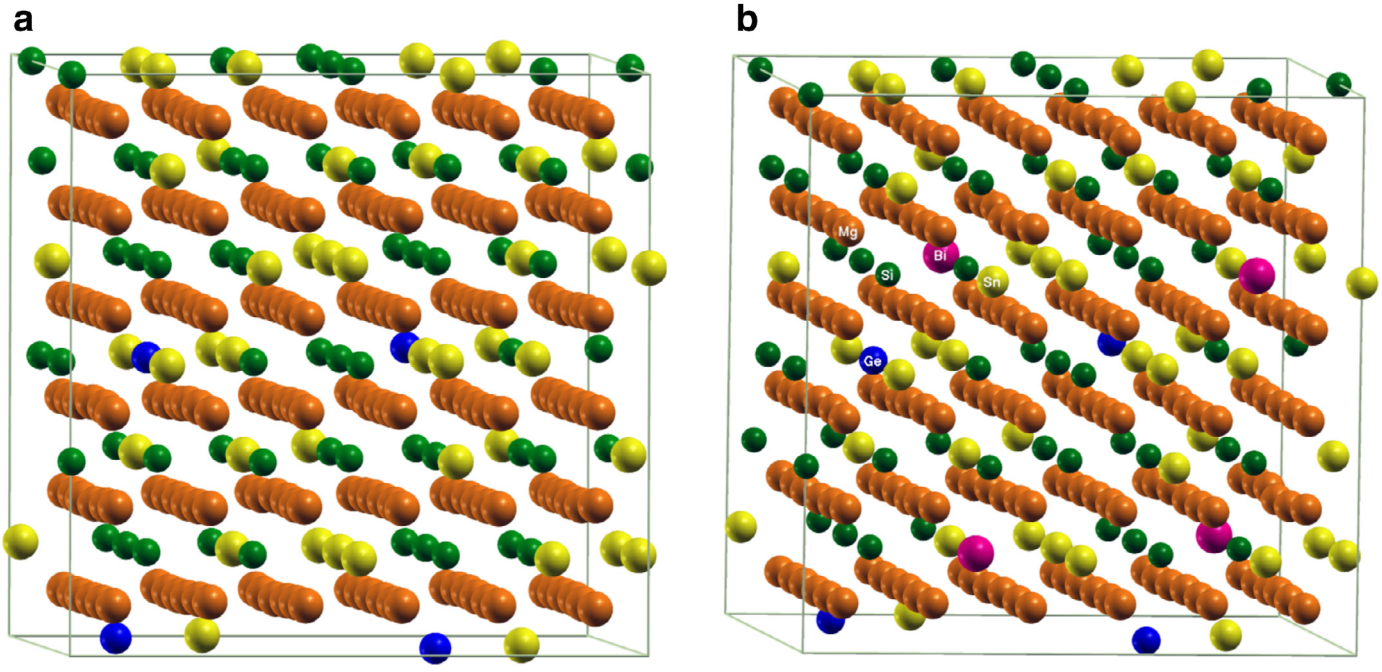

Fig. 1. Optimised atomic structures of (a) $Mg_2Si_{0.55}Sn_{0.4}Ge_{0.05}$ and (b) $Mg_2Si_{0.53}Sn_{0.4}Ge_{0.05}Bi_{0.02}$.

Table 1
Temperature variation of electrical and thermal transport properties of n-type doped semiconductors. Electronic transport properties are expressed as a function of Fermi integrals, $F_i = \int_0^\infty \frac{x^i dx}{e^{(x-\zeta^*)}+1}$ where $x = \frac{E}{k_B T}$ and $\zeta^* = E_f/k_B T$. Expressions for phonon relaxation rates from boundary scattering (τ_{qs}^{-1}(bs)), mass defect scattering (τ_{qs}^{-1}(md)), acoustic deformation scattering (τ_{qs}^{-1}(dp)), and anharmonic scattering (τ_{qs}^{-1}(anh)) are also included. More detailed discussions for thermal transport properties have been already given in Ref. [39].

Property	Expression
Fermi level	$E_f^{ext} = \frac{1}{2}(E_c + E_d) + \frac{k_B T}{2} \ln \frac{N_d}{2U_c} - k_B T \sinh^{-1}\left(\sqrt{\frac{U_c}{8N_d}} \exp(\frac{-\Delta E_i}{2k_B T})\right)$
Seebeck coefficient	$S = -\frac{k_B}{e}\left(\frac{(r+\frac{5}{2})F_{r+\frac{3}{2}}(\zeta^*)}{(r+\frac{3}{2})F_{r+\frac{1}{2}}(\zeta^*)} - \zeta^*\right)$
Electrical conductivity	$\sigma_{ext} = \frac{4}{3\pi\sqrt{\pi}} \frac{e^2}{m_c^*} \frac{\hbar \rho c_L^2}{E_D^2} F_{1/2} A T^{\varsigma}$
Carrier thermal conductivity	$\kappa_{el} = \left(\frac{k_B}{e}\right)^2 \sigma T \left(\frac{\left(r+\frac{7}{2}\right)F_{r+\frac{5}{2}}(\zeta^*)}{\left(r+\frac{3}{2}\right)F_{r+\frac{1}{2}}(\zeta^*)} - \left[\frac{\left(r+\frac{5}{2}\right)F_{r+\frac{3}{2}}(\zeta^*)}{\left(r+\frac{3}{2}\right)F_{r+\frac{1}{2}}(\zeta^*)}\right]^2\right)$
Bipolar thermal conductivity	$\kappa_{bp} = F_{bp} T^p \exp(-E_g/2k_B T)$
Phonon thermal conductivity	$\kappa_{ph} = \frac{\hbar^2 q_D^5}{6\pi^2 k_B T^2} \sum_s c_s^4 \int_0^1 dx x^4 \tau \bar{n}(\bar{n}+1)$ Phonon relaxation rates for scattering mechanisms: $\tau_{qs}^{-1}(bs) = \frac{c_s}{L}$ $\tau_{qs}^{-1}(\text{md}) = \frac{\Gamma_{\text{md}}\Omega}{4\pi c^3}\omega^4(qs)$ $\tau_{ql}^{-1}(\text{dp}) = \frac{3}{8\sqrt{\pi}} \frac{E_{df}^2}{\rho c_L^2 \hbar^4}(2m^* k_B T)^{3/2}$ $\tau_{qs}^{-1}(\text{anh}) = \frac{\hbar q_D^5 \gamma^2}{4\pi\rho c^2} \sum_{s's''\varepsilon}\left[\int dx' x'^2 x_+'' [(1-\varepsilon+\varepsilon(Cx+Dx')]\frac{\bar{n}_{q's'}(\bar{n}_+''+1)}{(\bar{n}_{qs}+1)} + \frac{1}{2}\int dx' x'^2 x_-'' [1-\varepsilon+\varepsilon(Cx-Dx')]\frac{\bar{n}_{q's'}\bar{n}_-''}{\bar{n}_{qs}}\right]$

Fig. 2 represents the electronic band structures of Mg_2Si, $Mg_2Si_{0.55}Sn_{0.4}Ge_{0.05}$ and $Mg_2Si_{0.53}Sn_{0.4}Ge_{0.05}Bi_{0.02}$, respectively. In agreement with the previously reported theoretical works [33,34] we predict the band gap value of 0.2 eV for Mg_2Si. This value is smaller than the experimental measured indirect band gap of in the range of 0.69 eV–0.78 eV [35]. It is a well known the fact that the accurate prediction of band gap in these systems is quite challenging since DFT within the LDA or the generalised gradient approximation (GGA) under estimates the band gaps of semiconductors due to factors such as self interactions. However, it is evident that comparing our band structures with other advanced approximations in DFT gives the same topology of the bands. From Figs. 2(b) and (c) it is clearly seen that when the Bi is doped

Table 2
Parameters required for thermoelectric transport computations of $Mg_2Si_{0.55-z}Sn_{0.4}Ge_{0.05}Bi_z$ solid solution series with the doping levels of z = 0.02, 0.025, 0.03, and 0.035.

Property/Parameter	z=0.02	z=0.025	z=0.03	z=0.035
$E_g(0)$ (eV) [40]	0.35	0.35	0.35	0.35
E_d (eV)	0.3	0.32	0.34	0.345
α (eV/K)	8.85×10^{-4}	8.85×10^{-4}	8.85×10^{-4}	8.85×10^{-4}
N_d (m^{-3}) [15]	2.2×10^{26}	3.0×10^{26}	3.8×10^{26}	4.2×10^{26}
m_n^*/m_e^*	0.37	0.466	0.52	0.53
m_p^*/m_e^*	0.407	0.512	0.572	0.583
r	1.5	1.5	1.5	1.5
ρ (kg/m^3) [41]	2.624×10^3	2.624×10^3	2.624×10^3	2.624×10^3
$\bar{c}$ (m/s) [42]	4.53×10^3	4.53×10^3	4.53×10^3	4.53×10^3
E_D (eV) [41]	8.513	8.513	8.513	8.513
A ($K^{-0.1}$)	1.2	1.55	1.7	1.6
a_{lat} (Å) [41]	6.51	6.51	6.51	6.51
ς	0.1	0.1	0.1	0.1
F_{bp} ($Wm^{-1}K^{-2}$)	0.001×10^{-4}	0.2×10^{-4}	0.002×10^{-4}	0.008×10^{-4}
q_D ($Å^{-1}$) [42]	0.95	0.95	0.95	0.95
L (mm)	10.0	10.0	10.0	10.0
Ω ($Å^3$) [43]	68.97	68.97	68.97	68.97
Γ_{md}	1.02	0.093	0.072	0.067
E_{df} (eV)	0.17	0.085	0.085	0.085
γ [44]	1.4	1.4	1.4	1.4

to $Mg_2Si_{0.55}Sn_{0.4}Ge_{0.05}$ solid solution the band topology is unchanged in $Mg_2Si_{0.53}Sn_{0.4}Ge_{0.05}Bi_{0.02}$ solid solution. In addition to that, as Bi has extra electrons it leads to an increase in the carrier concentration and pushes the extra electrons to some conduction bands causing a shift in the Fermi energy. Thereby, Bi doping makes the $Mg_2Si_{0.55}Sn_{0.4}Ge_{0.05}$ solid solution a degenerate semiconductor. From this result, it can be easily expected that Bi doping should cause a clear increment in the electrical conductivity due to the rising number of carrier concentrations.

Fig. 3(a) displays the theoretical calculations of temperature varied Fermi level for $Mg_2Si_{0.55-z}Sn_{0.4}Ge_{0.05}Bi_z$ solid solutions at 300 K $\leqslant T \leqslant$ 850 K. From our theoretical calculations it is found that our samples show only the extrinsic behaviour throughout the temperature range and they do not show the critical extrinsic-to-intrinsic turnover behaviour. This can be also easily verified from the experimental work of Khan et al. [15] from their Seebeck coefficient - T results. Additionally, as the Bi doping level increases E_F becomes larger due to increased concentration of donor impurity atoms, electron effective masses and donor energy levels (E_d), as listed in Table 2. Fig. 3(b) shows the Seebeck coefficient (S) as a function of temperature for $Mg_2Si_{0.55-z}Sn_{0.4}Ge_{0.05}Bi_z$ solid solutions along with their experimental values from Ref. [15]. For all Bi doped solid solutions $|S|$ increases nearly linearly with temperature as expected from the theoretical calculations of E_F - T we again do not observe any extrinsic-intrinsic turnover behaviour since they show only extrinsic behaviour in the studied temperature range. Moreover, the negative signs of S for all Bi doped samples confirm their n-type conduction with explaining that electrons are the main carriers of the electricity. Our theoretical computations suggest that the reason of having lower values of $|S|$ with increasing Bi doping level is

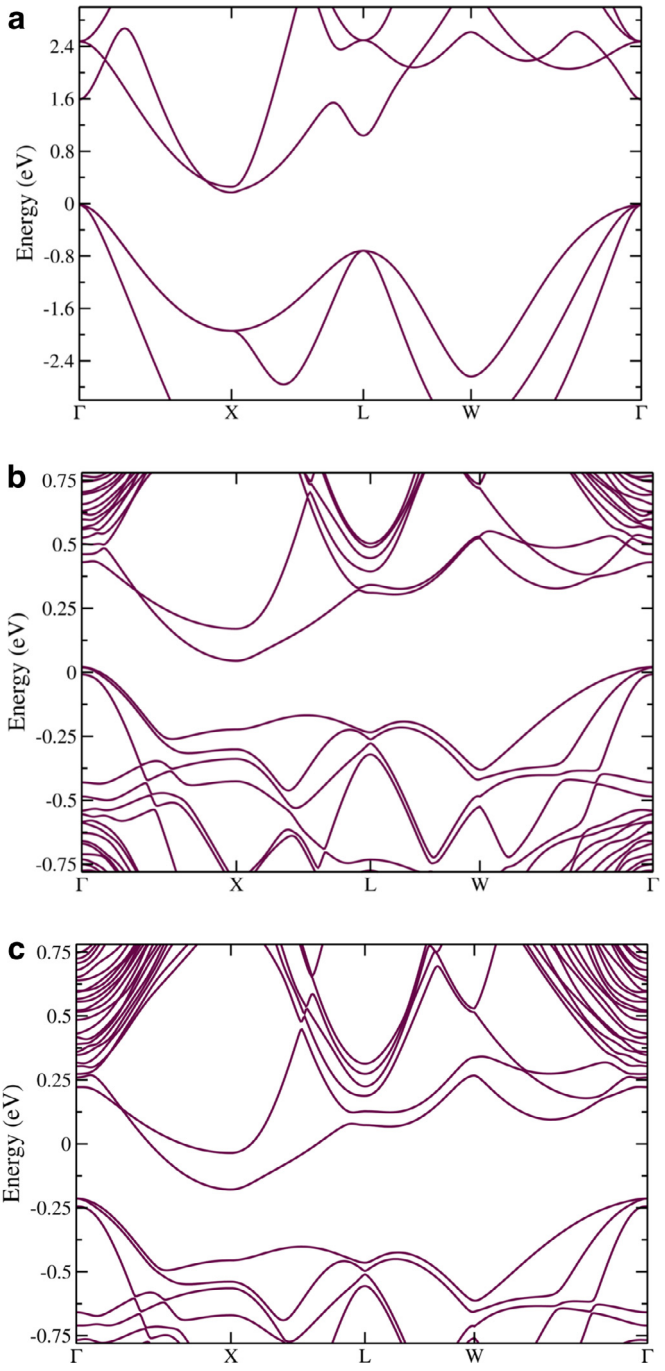

Fig. 2. Electronic band structures of (a) Mg_2Si, (b) $Mg_2Si_{0.55}Sn_{0.4}Ge_{0.05}$ and (c) $Mg_2Si_{0.53}Sn_{0.4}Ge_{0.05}Bi_{0.02}$. The Fermi level is set to zero.

because of increasing electron effective mass. Therefore, the highest S is attained for z=0.02 sample with the value of -211.0 μV/K at 850 K. Khan et al. also reported the maximum S as -216.86 μV/K at 804 K for the same sample [15]. Theoretical curves of electrical conductivity (σ) against temperature are plotted in Fig. 3(c) for $Mg_2Si_{0.55-z}Sn_{0.4}Ge_{0.05}Bi_z$ solid solutions including their experimental curves for comparison. For all type samples, σ decreases with increasing temperature which indicates that all samples show metallic like behaviour and their largest value obtained at room temperature. Khan

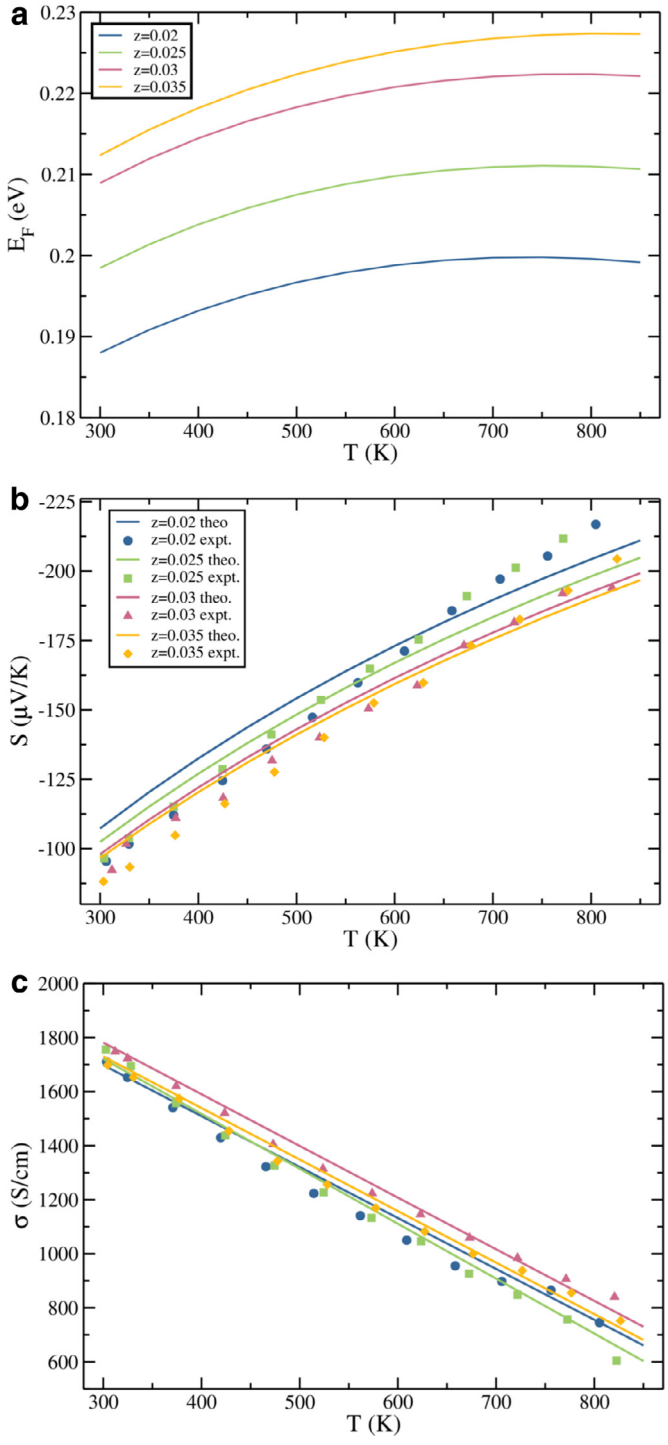

Fig. 3. Electrical transport properties of $Mg_2Si_{0.55-z}Sn_{0.4}Ge_{0.05}Bi_z$ series (z= 0.02, 0.025, 0.03, and 0.035) as a function of temperature. (a) Fermi level, (b) Seebeck coefficient, and (c) electrical conductivity. Theoretical analysis are represented with the solid lines and experimental data are shown as symbols read from Ref. [15].

et al. reported that the z=0.03 sample has higher electrical conductivity values for entire temperature range among other samples [15]. Therefore, to explain their results accurately we use the largest A parameter for z=0.03 sample as given in Table 2. Our theoretical result for the largest value of σ is in a

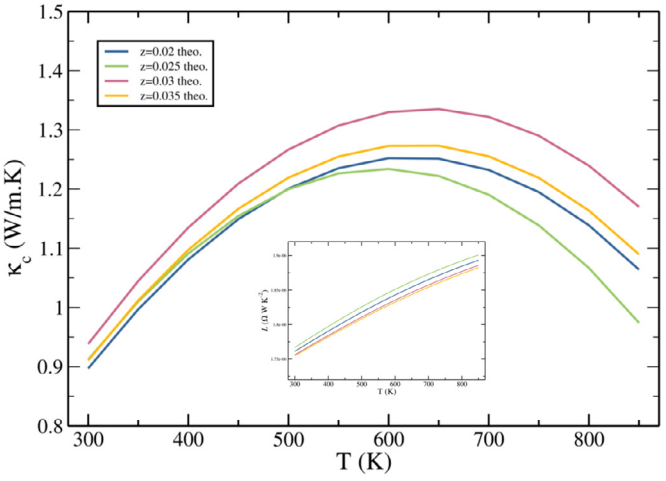

Fig. 4. Carrier thermal conductivity of $Mg_2Si_{0.55-z}Sn_{0.4}Ge_{0.05}Bi_z$ series (z= 0.02, 0.025, 0.03, and 0.035) as a function of temperature. The inset exhibits the temperature variation of the Lorenz number for Bi doping levels of quaternary series.

very good agreement with the work of Khan et al. [15]. While we found the (σ_{max}) as for z=0.03 sample with the value of 1781.36 S/cm at room temperature Khan *et al.* reported the value of 1747.84 S/cm at 312 K for the same sample [15]. When examining the electrical transport properties of S and σ in the view of both theoretically and experimentally it is seen that as the temperature increases while $|S|$ tends to raise the σ tends to decrease. This trend corresponds that all studied samples show highly doped semiconductor's behaviour.

Fig. 4 exhibits the carrier thermal conductivity (κ_c) of $Mg_2Si_{0.55-z}Sn_{0.4}Ge_{0.05}Bi_z$ solid solutions as a function of temperature. By taking into account of the Wiedemann Franz rule and the previous $\sigma - T$ dependence as it can be clearly anticipated we found that z=0.03 sample has higher κ_c values throughout the temperature range among other samples. The largest value of κ_c is calculated as 1.335 W/m.K at 650 K. In addition to that, the calculation of the temperature dependent Lorenz number ($\mathcal{L}$) is inserted as an inset in Fig. 4. We found that $\mathcal{L}$ shows a clear trend of increment as a function of temperature for all Bi doping levels. The highest $\mathcal{L}$ is gained for z=0.025 sample as 1.9×10^{-6} ΩWK^{-2} at 850 K which is significantly larger than its Sommerfeld value of $2.44\times10^{-8}\Omega WK^{-2}$.

Fig. 5(a) illustrates the sum of bipolar and lattice contribution - temperature variation for $Mg_2Si_{0.55-z}Sn_{0.4}Ge_{0.05}Bi_z$ solid solutions. First of all, it is clearly seen that our theoretical $\kappa_{bp} + \kappa_{ph}$ -T findings are in a fairly good agreement with the work of Khan et al. [15]. We want to primarily notice that for all Bi doping levels the bipolar contribution on thermal conduction starts to exhibit its visible effect nearly above 700 K and leads a very slight increment in $\kappa_{bp} + \kappa_{ph}$. Among all samples, from experimental findings it was reported that the z=0.025 sample has slightly sharper increase in $\kappa_{bp} + \kappa_{ph}$ above 700 K. This can be explained by using the highest F_{bp} parameter in our computations for z=0.025 sample as can be

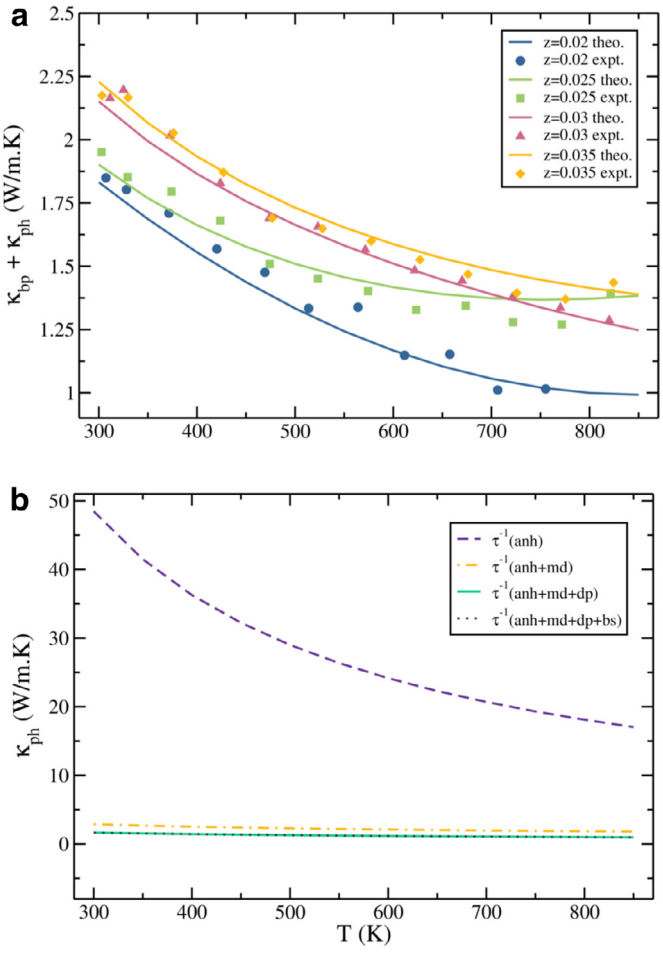

Fig. 5. (a) The combination of bipolar and lattice contribution on thermal conductivity changes with temperature for $Mg_2Si_{0.55-z}Sn_{0.4}Ge_{0.05}Bi_z$ series (z = 0.02, 0.025, 0.03, and 0.035). Theoretical analysis are represented with the solid lines and experimental data are shown as symbols read from Ref. [15]. (b) The influence of different scattering processes on lattice thermal conduction for $Mg_2Si_{0.53}Sn_{0.4}Ge_{0.05}Bi_{0.02}$ solid solution at different temperatures.

seen in Table 2. To obtain more detailed information about the temperature dependent phonon thermal conductivity the effect of different phonon scattering mechanisms on κ_{ph} is displayed for only z=0.02 sample in Fig. 5(b). We found that boundary scattering plays a major role on κ_{ph} below 100 K therefore its visible effect can not be seen in studied temperature range. Additionally, contributions from anharmonic and acoustic deformation potential scattering processes play a substantial role temperatures from 300 K to 850 K. However, more importantly, the mass defect scattering mechanism presents a dominant contribution for κ_{ph} among all other scattering processes. Now, we can go back to Fig. 5(a) and report that while the Bi doping level increases the value of $\kappa_{bp} + \kappa_{ph}$ becomes larger which can be explained with increasing mass defect parameter Γ_{md}. Furthermore, the smallest value of $\kappa_{bp} + \kappa_{ph}$ is attained both theoretically and experimentally for z=0.02 sample throughout the temperature range with the help of its larger mass defect scattering mechanism. While Khan et al. obtained the $(\kappa_{bp} + \kappa_{ph})_{min}$ as 1.01 W/m.K at 755 K [15] we found $(\kappa_{bp} + \kappa_{ph})_{min}$ as 0.99 W/m.K at 850 K. Binary undoped Mg_2Si has very large phonon thermal conductivity (11 W m^{-1} K^{-1}) at room temperature [36]. This value was decreased to 1.9 W m^{-1} K^{-1} at 300 K by using $Mg_2Si_{0.55}Sn_{0.4}Ge_{0.05}$ solid solution by Vlachos et al. [37] due to the incorporation of mass fluctuation via Si/Sn/Ge substitution. To achieve further decrease in phonon thermal conductivity the way of doping is tried for these quaternary systems since introducing additional atoms in lattice leads a significant increment of complexity in the systems' structure. For an effective n-type doping Bi is the best choice for Mg_2(SiGeSn) systems because Bi atom has heavier atomic weight than other possible atoms (i.e. As or Sb) which leads to stronger phonon scatterings with larger mass fluctuations [38]. Therefore, at room temperature, while the value of $\kappa_{bp} + \kappa_{ph}$ is 1.9 W m^{-1} K^{-1} for $Mg_2Si_{0.55}Sn_{0.4}Ge_{0.05}$ system [37] it is decreased to 1.83 W m^{-1} K^{-1} for our $Mg_2Si_{0.53}Sn_{0.4}Ge_{0.05}Bi_{0.02}$ sample. This reduction in $\kappa_{bp} + \kappa_{ph}$ becomes even more clear in higher temperatures; at 800 K, while the value is 2.1 W m^{-1} K^{-1} for $Mg_2Si_{0.55}Sn_{0.4}Ge_{0.05}$ system, our $Mg_2Si_{0.53}Sn_{0.4}Ge_{0.05}Bi_{0.02}$ sample has the value of 0.99 W m^{-1} K^{-1}. Moreover, percentage contribution from different polarisations of κ_{ph} is calculated for $Mg_2Si_{0.53}Sn_{0.4}Ge_{0.05}Bi_{0.02}$ solid solution. It is found that for throughout the temperature range heat is dominantly carried by transverse phonons and at room temperature the percentages are nearly 75.87% for transverse branch and 24.13% for longitudinal branch. Increasing temperature does not change this trend significantly.

The frequency variation of κ_{ph} carried by longitudinal and transverse branches for z=0.02 sample is displayed in Fig. 6 at several different temperatures. In Fig. 6(a) where only the longitudinal branch is included the κ_{ph} - frequency spectrum peaks at ω_D/5 at room temperature and ω_D/3.3 at 850 K (where ω_D is the Debye frequency which is 43.04 THz for $Mg_2Si_{0.55}Sn_{0.4}Ge_{0.05}$ alloy). Also, as the temperature increases the phonon-frequency spectrum forms wider and the peak slightly shifts to higher frequency which can be verified by dominant phonon approximation. In Fig. 6(b), the frequency dependence of κ_{ph} in which heat is considered to be carried only by transverse branch is presented for z=0.02 sample. The spectrum peaks at higher temperatures compared to previous calculation done for longitudinal branch. The κ_{ph} - frequency spectrum shows a peak at ω_D/3.07 for room temperature and at ω_D/2.22 for 850 K. Moreover, as observed in longitudinal phonons-frequency spectrum, the spectrum carried by transverse phonons forms broader with temperature.

Fig. 7 displays the total thermal conductivity κ_{total} of $Mg_2Si_{0.55-z}Sn_{0.4}Ge_{0.05}Bi_z$ solid solutions as a function of temperature. Increasing Bi doping level in $Mg_2Si_{0.55-z}Sn_{0.4}Ge_{0.05}Bi_z$ quaternary alloys leads simultaneous increase in κ_{total}. We notice that the z=0.02 sample has the lowest κ_{total} value throughout the temperature range with the help of its reasonably smaller $\kappa_{bp} + \kappa_{ph}$ value throughout the temperature range among other samples together with its very low κ_c value. The minimum value is theoretically attained as 2.05 W/m.K at 850 K whereas it was measured as 2.03 W/m.K at 803 K by Khan et al. [15].

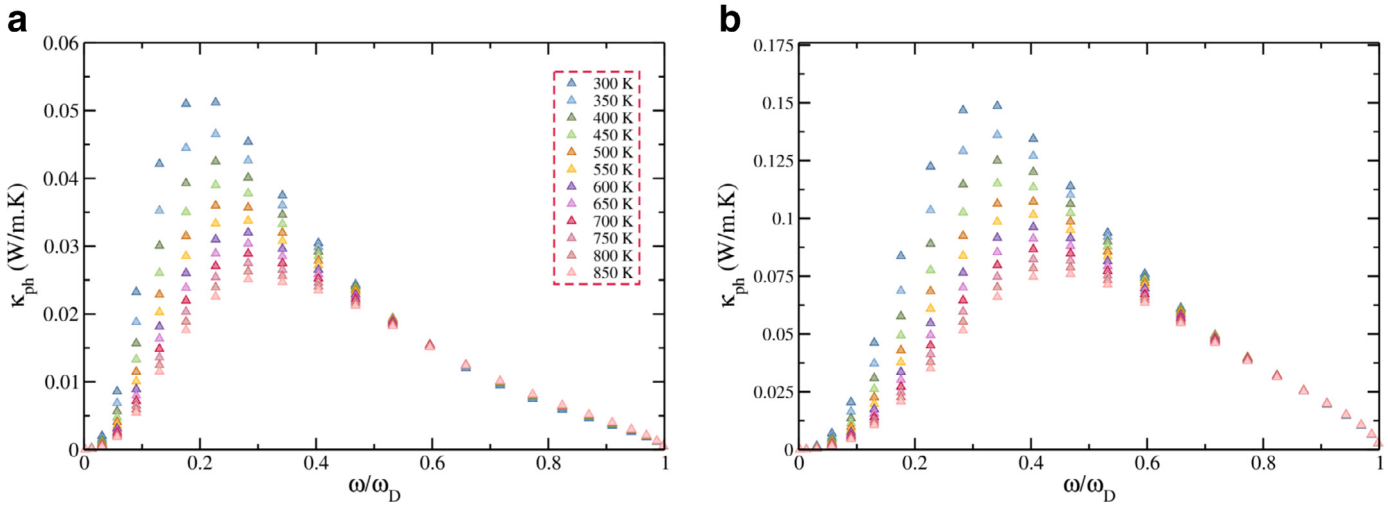

Fig. 6. Phonon thermal conductivity as a function of phonon frequency for $Mg_2Si_{0.53}Sn_{0.4}Ge_{0.05}Bi_{0.02}$ solid solution. (a) Only the longitudinal branch is included and (b) only the transverse branch is included. The Debye frequency is taken as ω_D=43.04 THz.

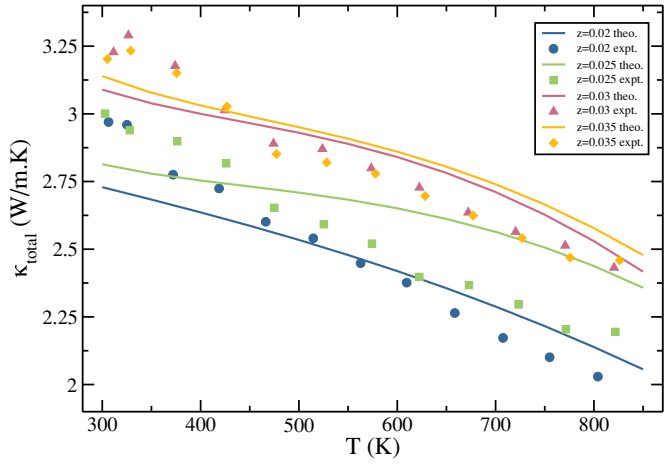

Fig. 7. Total thermal conductivity of $Mg_2Si_{0.55-z}Sn_{0.4}Ge_{0.05}Bi_z$ series (z = 0.02, 0.025, 0.03, and 0.035) as a function of temperature. Theoretical analysis are represented with the solid lines and experimental data are shown as symbols read from Ref. [15].

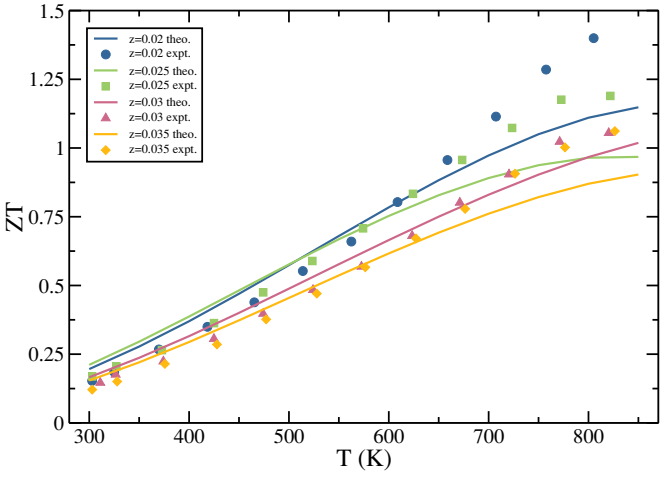

Fig. 8. Dimensionless thermoelectric figure of merit of ZT of $Mg_2Si_{0.55-z}Sn_{0.4}Ge_{0.05}Bi_z$ series (z = 0.02, 0.025, 0.03, and 0.035) as a function of temperature. Theoretical analysis are represented with the solid lines and experimental data are shown as symbols read from Ref. [15].

In Fig. 8, we display how the dimensionless figure of merit (ZT) of $Mg_2Si_{0.55-z}Sn_{0.4}Ge_{0.05}Bi_z$ series varies with temperature including their related experimental values. Interestingly, while the z=0.02 sample has lower electrical conductivity for entire temperature range it presents the largest ZT which is owing to its significantly larger $|S|$ value and its smaller κ_{total} value. The maximum ZT value for this level of Bi doped solid solution is calculated to be 1.14 at 850 K whereas in the work of Khan et al. [15] they measured its value as 1.4 at 805 K.

4. Conclusions

In this work, we reported thermoelectric transport behaviours changes with temperature for n-type $Mg_2Si_{0.55-z}Sn_{0.4}Ge_{0.05}Bi_z$ solid solutions with the doping levels of z=0.02, 0.025, 0.03, and 0.035. We can list our theoretical outcomes as;

- Samples with all different Bi doping levels display extrinsic behaviour entire temperature range.
- Increasing the Bi doping level causes a clear reduction in the Seebeck coefficient owing to raising electron effective mass.
- The highest S is attained for z=0.02 sample with the value of -211.0 μV/K at 850 K.
- The maximum σ is found for z=0.03 sample as 1781.36 S/cm.
- The minimum κ_{total} is found for z=0.02 sample due to its smaller $\kappa_{bp} + \kappa_{ph}$ value.
- The maximum ZT is attained for z=0.02 doping level as 1.14 at 850 K because of its higher S and lower $\kappa_{bp} + \kappa_{ph}$ values.

To summarize, being different from previous works, our Bi doped Mg_2(Si,Sn,Ge) quaternary systems are studied in detail

theoretically by including their temperature dependent Fermi level to understand their extrinsic semiconductor behaviour and their thermal conductivity contributions from electron-hole pairs and phonons including all required phonon scattering mechanisms rigorously. Having higher dimensionless thermoelectric figure of merits for our quaternary Mg_2(Si,Sn,Ge) solid solution series is mainly due to the effect of additional atoms which cause a reduction in phonon thermal conductivity. Moreover, Bi atom seems to be more efficient dopant than Sb atom for n-type Mg_2(Si,Sn,Ge) series to have better thermoelectric efficiencies.

Declaration of Competing Interest

This piece of the submission is being sent via mail.

Acknowledgement

Övgü Ceyda Yelgel wishes to acknowledge financial support from TÜBİTAK (Scientific and Technical Research Council of Turkey) (Project number: 115F387).

References

[1] L.E. Bell, Science 321 (2008) 1457.
[2] C. Wood, Rep. Prog. Phys. 51 (1988) 459.
[3] G.J. Snyder, E.S. Toberer, Nat. Mater. 7 (2008) 105.
[4] D. Kraemer, B. Poudel, H.P. Feng, J.C. Caylor, B. Yu, X. Yan, Y. Ma, X. Wang, D. Wang, A. Muto, K. McEnaney, M. Chiesa, Z. Ren, G. Chen, Nat. Mater. 10 (2011) 532.
[5] G.S. Nolas, J. Sharp, H.J. Golsmid, Thermoelectrics Basic Principles and New Materials Developments, Springer, Germany, 2001.
[6] S.K. Bux, M.T. Yeong, E.S. Toberer, G.J. Snyder, R.B. Kaner, J.P. Fleurial, J. Mater. Chem. 21 (2011) 12259.
[7] R. Saravanana, M.C. Robert, J. Alloys Compd. 479 (2009) 26.
[8] V.K. Zaitsev, M.I. Fedorov, E.A. Gurieva, I.S. Eremin, P.P. Konstantinov, A.Y. Samunin, M.V. Vedernikov, Phys. Rev. B 74 (2006) 045207.
[9] Q. Zhang, J. He, T.J. Zhu, S.N. Zhang, X.B. Zhao, T.M. Tritt, Appl. Phys. Lett. 93 (2008) 102109.
[10] G.J. Snyder, E.S. Toberer, Nat. Mater. 7 (2008) 105.
[11] R.D. Redin, R.G. Morris, G.C. Danielson, Phys. Rev. 109 (1958) 1916.
[12] B.D. Lichter, J. Electrochem. Soc. 109 (1962) 819.
[13] R.J. LaBotz, D.R. Mason, D.F. O'Kane, J. Electrochem. Soc. 110 (1963) 127.
[14] W. Liu, X.J. Tan, K. Yin, H.J. Liu, X.F. Tang, J. Shi, Q.J. Zhang, Phys. Rev. Lett. 108 (2012) 166601.
[15] A.U. Khan, N.V. Vlachos, E. Hatzikraniotis, G.S. Polymeris, C.B. Lioutas, E.C. Stefanaki, K.M. Paraskevopoulos, I. Giapintzakis, T. Kyratsi, Acta Mater. 77 (2014) 43.
[16] M. Akasaka, T. Iida, A. Matsumoto, K. Yamanaka, Y. Takanashi, T. Imai, N. Hamada, J. Appl. Phys. 104 (2008) 013703.
[17] H. Wang, W. Chu, H. Jin, Comput. Mater. Sci. 60 (2012) 224.
[18] N. Satyala, D. Vashaee, J. Electron. Mater. 41 (2012) 1785.
[19] X.J. Tan, W. Liu, H.J. Liu, J. Shi, X.F. Tang, C. Uher, Phys. Rev. B 85 (2012) 205212.
[20] J.J. Pulikkotil, D.J. Singh, S. Auluck, M. Saravanan, D.K. Misra, A. Dhar, R.C. Budhani, Phys. Rev. B 86 (2012) 155204.
[21] K. Kutorasinski, J. Tobola, S. Kaprzyk, Phys. Rev. B 87 (2013) 195205.
[22] J. Tani, H. Kido, Phys.a B 364 (2005) 218.
[23] T. Yi, S. Chen, S. Li, H. Yang, S. Bux, Z. Bian, N.A. Katcho, A. Shakouri, N. Mingo, J.P. Fleurial, N.D. Browning, S.M. Kauzlarich, J. Mater. Chem. 22 (2012) 24805.
[24] Ö.C. Yelgel, G.P. Srivastava, Phys. Rev. B 85 (2012) 125207.
[25] L.D. Hicks, M.S. Dresselhaus, Phys. Rev. B 47 (1993) 12727.
[26] P.J. Price, Phil. Mag. 46 (1955) 1252.
[27] P. Giannozzi, S. Baroni, N. Bonini, M. Calandra, R. Car, C. Cavazzoni, D. Ceresoli, G.L. Chiarotti, M. Cococcioni, I. Dabo, A.D. Corso, S. Fabris, G. Gougoussis, A. Kokalj, M. Lazzeri, L. Martin-Samos, N. Marzari, F. Mauri, R. Mazzarello, S. Paolini, A. Pasquarello, L. Paulatto, C. Sbraccia, S. Scandolo, G. Sclauzero, A.P. Seitsonen, A. Smogunov, P. Umari, R.M. Wentzcovitch, J. Phys.: Condens. Matter 21 (2009) 395502.
[28] J.P. Perdew, A. Zunger, Phys. Rev. B 23 (1981) 5048.
[29] H.J. Monkhorst, J.D. Pack, Phys. Rev. B 13 (1976) 5188.
[30] M. Methfessel, A. Paxton, Phys. Rev. B 40 (1989) 3616.
[31] E. Owen, G. Preston, Proc. Phys. Soc. Lond. 36 (1923) 341.
[32] C.J. Glassbrenner, G.A. Slack, Phys. Rev. 134 (1964) A1058.
[33] A.V. Krivosheeva, A.N. Kholod, V.L. Shaposhnikov, A.E. Krivosheev, V.E. Borisenko, Semiconductors 36 (2002) 496500.
[34] H. Balout, P. Boulet, M.C. Record, J. Electron. Mater. 42 (2013) 34583466.
[35] H. Wang, W. Chu, H. Jin, Comput. Mater. Sci. 60 (2012) 224.
[36] M. Ioannou, K. Chrissafis, E. Pavlidou, F. Gascoin, T. Kyratsi, J. Solid State Chem. 197 (2013) 172e180.
[37] N. Vlachos, G.S. Polymeris, M. Manoli, E. Hatzikraniotis, A.U. Khan, C.B. Lioutas, E.C. Stefanaki, E. Pavlidou, K.M. Paraskevopoulos, J. Giapintzakis, T. Kyratsi, J. Alloy. Comp. 714 (2017) 502.
[38] A.U. Khan, N. Vlachos, T. Kyratsi, Scripta Materilia 69 (2013) 606.
[39] O.C. Yelgel, Philos. Mag. 96 (6) (2016) 560.
[40] V.K. Zaitsev, M.I. Fedorov, I.S. Eremin, E.A. Gurieva, Thermoelectrics Handbook: Macro to Nano Structured Materials, CRC Press, New York, 2005. Ch. 29
[41] J.-H. Bahk, Z. Bian, A. Shakouri, Phys. Rev. B 89 (2014) 075204.
[42] D.R. Lide, CRC Handbook of Chemistry and Physics, 87th, Taylor and Francis Group LLC, 2007.
[43] P. Pandit, P.S. Sanyal, Indian J. Pure Appl. Phys. 49 (2011) 692.
[44] H. Wang, H. Jin, W. Chu, Y. Guo, J. Alloys Comp. 499 (2010) 68.